International Journal of Physics
and Research (IJPR)
ISSN(P): 2250-0030; ISSN(E): 2319-4499
Vol. 5, Issue 4, Aug 2015, 29-38

EFFECT OF GRAPHENE / MONTMORILLONITE ON CHITOSAN NANOCOMPOSITES WITH MODIFIED MORPHOLOGY, THERMAL AND ELECTRICAL PROPERTIES

SUCHISMITA MOHANTY[1], SUBRATA SARANGI[2] & GOURI SANKAR ROY[3]

[1,2]Department of Physics, Centurion University of Technology and Management, Odisha, India

[3]Research Scholar, Department of Physics, College of Engineering and Technology,
Bhubaneswar, Odisha, Khordha, India

ABSTRACT

Polymer composites, filled by graphitic nanostructures, have attracted increased attention owing to their unique thermal and electric properties. In this study, grapheme / montmorillonite / chitosan (GE/MMT/CS) was prepared by a simple solution mixing-evaporation method. The effects of GE/MMT /CS on thermal and electrical properties of the nanocomposite films were investigated. The results indicate that the simultaneously introduced GE and MMT into CS could greatly improve the physical properties. Thermal analysis of the samples shows that the material is stable up to 230°C and maintains its thermal stability all throughout the process until it starts degrading after 480°C. Investigations of electrical properties of CS/MMT/GE show a significant increase of electrical conductivity with the increase of the GE content. The conductivity of the sample with only 5 wt% GE load is as high as 10^{-2} S/cm which is four orders of magnitude higher than that of the neat polymer.

KEYWORDS: Nanocomposites, Chitosan, Graphene, Themal and Electrical Properties

INTRODUCTION

The concept of charge storage within the electrochemical double layer was first described by the German Physicist Hermann von Helmholtz in 1858 [1]. However, it took another 100 years before this principle was used for energy storage applications. The first reference of a EDLC-like energy storage device dates back to a patent by General Eclectics in 1957, describing a "Low voltage electrolytic capacitor"[2]. Graphene, since its discovery in 2004 [3] has continued to gain significance owing to its extremely attractive characteristics. The first observation of a graphene-like structure was made by Boehm et al. in 1962. They used electron microscopy to investigate so called "graphite oxide soot" [4], which was derived from degradation of graphite oxide. The electron microscope revealed the soot to consist of thin packages of carbon hexagonal sheets today referred to as "graphene nanoplatelets"[5]. However, at that time the response of the scientific community was limited and thus, no further studies were conducted in this direction. In the meantime, graphite and graphite intercalation compounds attracted great interest, as they ordered a feasible way for ion storage [6-10]. Hence, as part of providing the terminology for graphite intercalation compounds in 1994, Boehm et al. introduced the term of "graphene" describing a single carbon layer of the graphite structure [11]. In order to bestow the conductivity in exfoliated graphene oxide, it had to be stripped off the oxygen functionalities that make them highly hydrophilic allowing intercalation of water molecules. In other words, Graphene Oxide has highly disoriented sp^2 bonding due to the presence of

oxygen atoms that randomly bond to graphene sites and convert them to sp^3 carbon bonds eventually making them electrically insulative [12]. So, in order to render them with properties similar to those of Graphite, the sp^2 configurations have to be restored.

Chitosan is one of the promising natural polymers with characteristics such as biodegradability, chemical inertness, biocompatibility, high mechanical strength, good film-forming properties, and low cost [13]. However, in sensor applications, the poor electrical conductivity of hydrogels results in a poor response time and a high operational voltage limits its applicability in devices. Hence, composites have been attempted by incorporating a rigid conducting polymer (such as PANI) into a flexible matrix (such as chitosan) to combine the good processability of the matrix and the electrical conductivity of the conductive polymer [14,15].

Polymer/layered silicate nanocomposites frequently exhibit remarkably improved mechanical and materials properties (such as a higher modulus, increased strength, decreased gas permeability and increased biodegradability of biodegradable polymers), and are attracting considerable interest in the polymeric materials field [16]. Na+-montmorillonite (MMT) is one of the most important layered silicates used for the preparation of these organicinorganic nanocomposites. MMT is composed of an aluminate sheet sandwiched between two silicate sheets stacked together by weak ionic and vander Waals forces which make MMT easily to be intercalated and/or exfoliated [17]. Swelling ratio and mechanical behavior of the poly (N-isopropylacrylamide) hydrogel were improved by the introduction of MMT [18]. The $–NH_2$ groups of CS are protonated in acidic aqueous solution and could intercalate into layers of MMT to form the CS/MMT nanocomposites . The CS/MMT nanocomposite film was seldom investigated until now although the CS/MMT systems have been applied in many fields [18].

In the present work, the GE/MMT/CS nanocomposite have been prepared by introducing MMT and GE into neat CS through a simple solution-evaporation method, and the synergistic effects on the thermal and electrical properties of nanocomposite are investigated. The positively charged polymeric chains of CS could intercalate into layers of MMT through a cation exchange process and cause the exfoliation of the weakly linked MMT sheets. The positively charged polymeric chains of CS could adsorb onto the surface of GE and act as polymeric cationic surfactants in acidic medium. Figure1. Schematically shows the synergistic effect of MMT and GE.

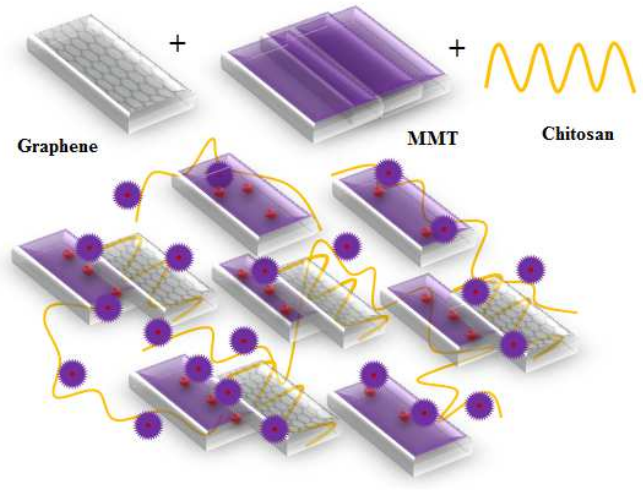

Figure 1: Schematic Structure of the GE/ MMT/ CS Nanocomposite

EXPERIMENTAL

Materials

CS was supplied by Himedia. MMT with a cation-exchange capacity of 102.8 mmol/100 g was supplied by sorthen clay USA. Graphene were purchased from Redex Nano Lab, UP India. The catalyst in the GE was removed by concentrated nitric acid, and then filtered and washed with double-distilled water until pH > 5. All solutions were prepared with doubledistilled water.

Preparation of the CS/MMT/GE Nanocomposite Films

The GE/ MMT/CS nanocomposite films were prepared according to the following procedure. 5 g of CS was dissolved in 200 ml of the aqueous solution of acetic acid (2% v/v). Appropriate amount of MMT and GE were suspended in 8.0 ml double-distilled water with sonication for 30 min at 25°C, 40 kHz and 100 W. CS was charged into the MMT/GE mixture and mechanically stirred at 1000 rpm for 1h followed by 30 min at 12 000 rpm, and then sonicated for 20 min to facilitate the intercalation of MMT and the dispersion of GE. After that, the GE/ MMT/ CS mixture was poured into a glass dish (7 cm×13 cm) and the water was evaporated at 45°C. The uniform nanocomposite films with an average thickness of 40 μm were then obtained and no further treatment was employed. The weight ratio of MMT and GE (mMMT: mGE = 1:1) to the total solid is kept at 0, 0.2, 0.5, 1.0, 2.0 and 5.0 wt%. The CS/MMT and CS/GE nanocomposite films were prepared according to the same procedure. The weight ratio of MMT or GE to the total solid is kept at 0, 0.2, 0.5, 1.0, 2.0 and 5.0 wt% [20].

Characterization

XRD

X-ray diffraction (Rigaku, D/Max, 2,500 V, Cu-αa radiation: 1.54056 A) experiments were carried out on both the plain PAA and the composite samples.Wide-angle X-ray diffractograms were recorded at temperature of 30^0C after isothermal crystallization at this temperature for 1 h.

IR Spectra

The Fourier transform infrared (FT-IR) spectra were recorded on a Nicolet 8700 spectrometer, in the range 400–4,000 cm^{-1}.

TEM

TEM experiments were performed on a Hitachi H-8100 electron microscope with an accelerating voltage of 200 kV.

Thermal Stability

The thermal stability of the sample was carried out using a thermogravimetric analyzer (Q5000 IR/SDT Q600-TA-Instrument, Seoul, Korea) programmed at a heating rate of 5 °C/min in the presence of air.

Dielectric Spectroscopy

AC dielectric spectroscopy was performed with a dielectric spectrometer BDS-80 (Novocontrol) equipped with a Hewlett Packard 4291B probe head operating in the frequency range of 106 to 1.8X109 Hz. Samples with a diameter of 10 mm and thicknesses ranging from 1 - 4 mm were placed in the holder between two parallel gold-plated electrodes (10 mm

in diameter). All experiments were carried out at a constant temperature of 25 °C – the sample holder was placed in a cryostat that enables the control of the temperatures with an accuracy of 0.1 °C. Prior to each test, a 30 min. time interval was applied in order to achieve temperature equilibrium. Novocontrol Win DETA software was used for the evaluation of the electrical properties of the samples. Complex permittivity and conductivity were calculated and plotted as a function of the frequency.

RESULTS AND DISCUSSIONS

XRD

XRD patterns of CS, MMT and GE are shown in Figure 2. As can be seen, in these XRD technique is the best and accurate analytical method. The X-ray diffraction pattern of pure Chitosan. The XRD analysis was used to study the crystalline of the prepared samples. The peaks at 2θ=20° for pure chitosan confirms the semi crystalline nature [21]. The typical diffraction peak of MMT is observed at 2 θ = 7.92° corresponding to a basal spacing of 1.272 nm, whereas, CS and GE show no diffraction peak in the 2θ range investigated. The peak of graphene at 2θ =30^0 was decreased in its intensity and broadened in its width, and enlarged slightly due to intercalate reaction but still kept the planar stacking structure. Further, the mixed phased (CS/MMT) high intensity peaks are attributed. XRD patterns of GE/MMT/CS composites change dramatically in comparison with CS, GE, CS/MMT and MMT. All diffraction peaks shift toward lower angle values, become broad, and even disappears, indicating that intercalation or exfoliation structures have been formed [22].

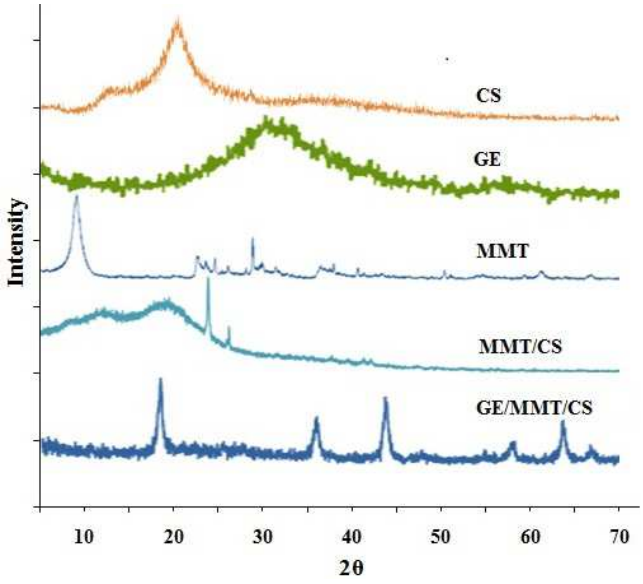

Figure 2: XRD Patterns of CS, MMT, GE, GE/CS and CS/GE/MMT Nanocomposite

FTIR

Figure 3 illustrates the FTIR spectra of MMT, CS, GE and GE/MMT cross-linked CS nanocomposite. The IR spectrum of the MMT show to peaks, which correspond to Si-O stretching at 1112 cm^{-1} and interlayer water deformation vibrations at 1636 cm^{-1} [23].The band at 3620 cm^{-1} results from the O-H stretching vibration and chitosan has strong peaks observed at 3454cm^{-1} due to OH group and the bands at 2923.08cm^{-1} and 1021.37cm^{-1} may be due to C-H stretching vibration and C-O-C stretching vibrations respectively [24]. The GE synthesis is successful with the support of FT-IR characteristic peaks O-H stretching vibrations observed at 3400 cm^{-1} was significantly reduced due to deoxygenating.

However, stretching vibrations from C=O at 1720 cm^{-1} were still observed and C-O stretching vibrations at 1060 cm^{-1} became sharper [25]. When comparing FTIR results between GE and GE/MMT cross-linked CS, the locations of basic peaks of C H stretching (2860 cm^{-1}), C- O -C stretching (1020 cm^{-1}), hydrogen bonds (3300–3600 cm^{-1}) and C= O stretching (1636 cm^{-1}) in –NHCO- are similar. The reaction between MMT groups and amino groups transforms primary amine groups (-NH_2) into secondary amine groups (NH) which also has similar peaks [26]. However, the close examination of FT-IR results illustrates that the intensity of C=O stretching of –NHCO- (the un-deacetylation units) declines and the N- H bending demonstrates the blue shift from 1538 cm^{-1} to 1532 cm^{-1}.Therefore, the results of FT-IR are consistent with the gel content test both of which indicate the cross-linking reaction between GE/MMT and CS.

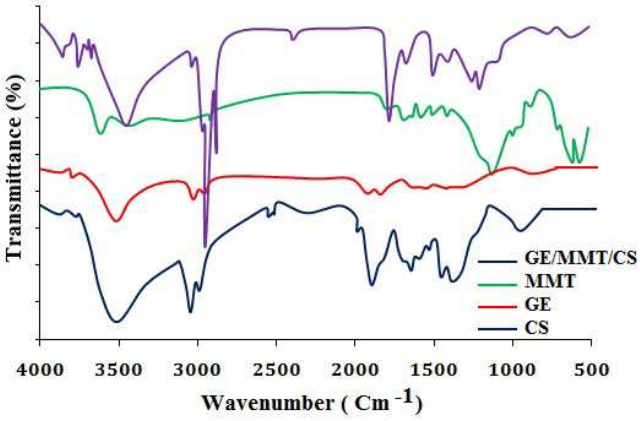

Figure 3: FTIR Spectrum of CS, MMT and GE/MMT/CS

SEM

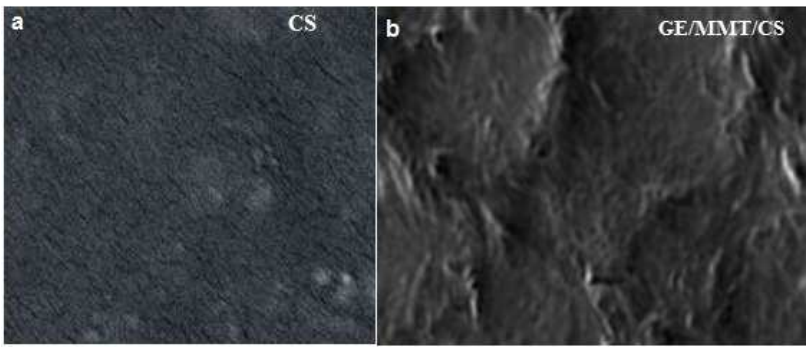

Figure 4: SEM of CS and GE/MMT/CS

Figure 4 shows SEM images of the fracture surfaces of the neat CS and the GE/MMT/CS nanocomposite. As shown in Figure 4a, the neat CS shows a smooth and tight fracture surface. An almost homogeneous dispersion of MMT and GE is observed throughout the CS matrix as shown in Figure 4b except for some small aggregates of MMT on the top of the graph. Consequently, an effective three-dimensional network is constructed and the CS/MMT/GE nanocomposite is formed with MMT and GE as inorganic crosslinkers. It can also be seen from homogeneously dispersed MMT and GE, which may be attributed to their strong interfacial interaction with the CS matrix [27, 28].

TGA and DSC

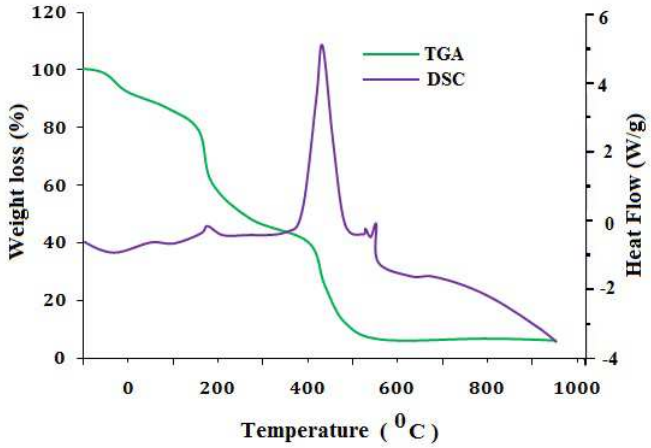

Figure 5: Thermographs of GE/CS/MMT Nanocomposite

Thermal analysis of the sample was carried out to assess the stability of the material at higher temperatures and to understand its degradation behavior during extreme physical conditions in a thermal application if used in any form. The thermographs are shown in Figure 5. From the figure, it is evident that the material is extremely stable until 250 °C, which is later followed by step-wise weight loss of the sample owing to the degradation of chitosan at the initial stages. The initial drop in weight before 150 °C is majorly attributed to the removal of moisture, carboxylic and hydroxyl groups from chitosan; from there onwards, the complete degradation starts, owing to 50% of the weight loss of the sample. On further heating to ~260 °C, the organic moieties of the saccharide rings get completely denatured. The presence of strong exothermic peaks arising around 500–600 °C for all of the samples is attributed to the degradation. On further heating above 700 °C, the weight loss of almost 97% reflects the degeneration of the graphene structure. As is observed from the functionalized composite thermogram, these cross-linkages have increased the thermal capacity and elasticity of the material [29].

Dielectric Spectroscopy

In this study, dynamic dielectric measurements have been performed in a frequency range of 1 MHz – 1.8 GHz. Figure 6a shows the real part of the dielectric permittivity as a function of frequency for GE/MMT composites with weight ratio of MMT and GE. In general, ε’ increases with an increase of weight of ratio in the entire frequency range. However, this increase is more pronounced at lower frequencies. The real part of the dielectric permittivity of the 5 wt% composite is two orders of magnitude higher than that of neat polymer at 1 MHz; and ε’ changes by a factor of 10 at 1 GHz. The increase of ε’ is related to the formation of mini-capacitors in composites, which gives rise to polarization.

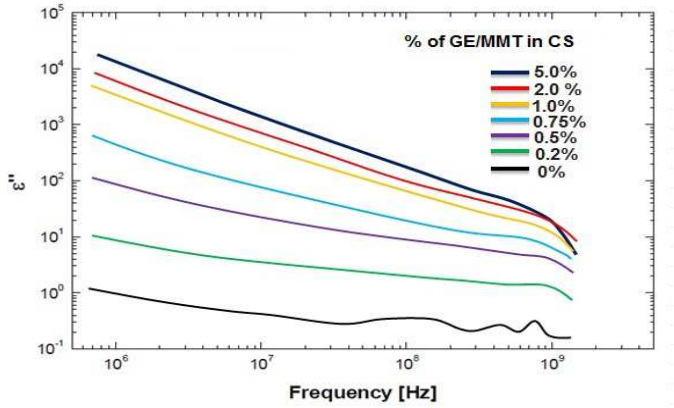

Figure 6a: Real Permittivity (ε') of CS/GE/MMT Composites versus Frequency

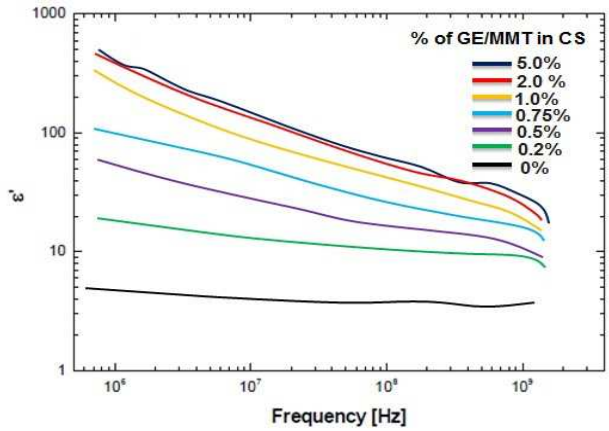

Figure 6b: Imaginary Permittivity (ε'') of MWNT/PDDA Composites versus Frequency

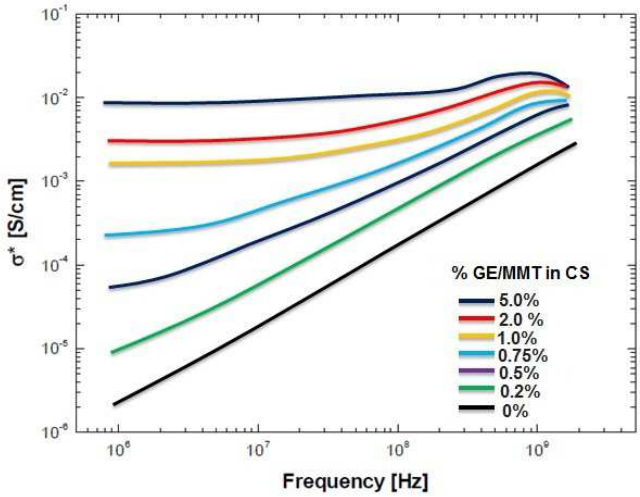

Figure 6c: Complex conductivity (ε *) of MWNT/PDDA Composites versus Frequency

Neat polymers display behavior of ε' being nearly independent of frequency. A similar trend is observed for samples with low GE concentrations (e.g. 0.5 wt %). When the GE/MMT content increases the behavior of ε' changes following the frequency dependent relation $\varepsilon' = \omega^{-u}$ (where u is a fitting parameter), which denotes the decreasing trend of ε' as the frequency increases. Table 1 shows the values of the scaling exponent u. The imaginary dielectric permittivity ε'' as a function of frequency (Figure 6b), exhibits similar dependence on the concentration of GE/MMT in the nanocomposite. However, above a concentration of 2 wt%, ε'' shows a much higher increase of the values than the real

permittivity ε'. At 1 MHz the imaginary permittivity is four orders of magnitude higher as the graphene concentration increases from 0 to 5 wt%; at 1.8 GHz it changes by a factor of 100. In general, the dielectric constant has been reported to dramatically increase with higher loading of GE/MMT above the percolation threshold, but at the expense of rapidly increasing dielectric loss (ε''). The large increase of dielectric loss above the percolation threshold is directly related to the DC conductivity $\sigma_{DC}=\omega\varepsilon''$ that appears in the percolated network at frequencies below the critical point at which the conductivity changes its behavior from frequency dependent to independent (where σ* comes into a plateau region - Figure 6c). Therefore, above the percolation threshold, when conductive paths are formed, ε'' increases rapidly, because the DC conductivity becomes dominant in electrical response of the samples [30-32].

Table 1: Fitting Parameters s and u for Composites with Different wt% of GE

	Wt% of GE/MMT in CS					
	0	**0.2**	**0.5**	**1**	**2**	**5**
σ* power law dependence ($\sigma^* \propto \omega^s$) value of s	0.91	0.82	0.73	0.62	0.51	0.45
ε' power law dependence $\varepsilon' \propto \omega^{-u}$) value of u	0.03	0.15	0.28	0.31	0.47	0.50

These results emphasize one important issue: the fabrication of composites with a high dielectric constant but with low losses can be achieved by efficient separation of the individual conductive particles in a polymer matrix. Thus, DC conductivity can be preserved, which diminishes its contribution to the increase of the imaginary part of the dielectric constant. Well separated conductive inclusions act as capacitors, giving rise to higher values of ε'.

CONCLUSIONS

The novel GE/MMT/CS nanocomposite films were successfully prepared by the simple solution-evaporation method. The synergistic effect of MMT and GE on mechanical properties of the nanocomposite is obviously observed. The $-NH_3^+$ groups of CS wrapped on the surface of GE could interact with the negative charged MMT sheets and form the MMT CS GE subassembly which may be responsible for the synergistic effect of MMT and GE on thermal and electrical properties of the neat CS. The introduction of two functional additives with different properties and structure for the improvement of material's properties may be applicable to other materials.

REFERENCES

1. P. Kurzweil, history | electrochemistry, Reference Module in Chemistry, Molecular Sciences and Chemical Engineering, from Encyclopedia of Electrochemical Power Sources, 2009, 533-554.
2. Pawan Sharma, T. S. Bhatti A review on electrochemical double-layer capacitors, Energy Conversion and Management, 2010, 51 (12), 2901-2912.
3. Kalyan Raidongia, Alvin T. L. Tan, Jiaxing Huang, Chapter 14 - Graphene Oxide: Some New Insights into an Old Material, Carbon Nanotubes and Graphene (Second Edition), 2014, 341-374
4. Franziska Schäffel Chapter 2 - The Atomic Structure of Graphene and Its Few-layer Counterparts, Graphene, 2013, 5-59
5. S. Stankovich, R. D. Piner, S. T. Nguyen, and R. S. Ruo_, Synthesis and exfoliation of isocyanate-treated graphene oxide nanoplatelets, Carbon, 2006, 443342.

6. F. Lincoln Vogel, The electrical conductivity of graphite intercalated with superacid uorides: experiments with antimony pentauoride, J. Mater. Sci. 1977, 12, 982.
7. J. O. Besenhard, E. Theodoridou, H. M ohwald, and J. J. Nickl, Electrochemical applications of graphite intercalation compounds, Synth. Met. 1982, 4, 211 .
8. R. Fong, U. von Sacken, and J. R. Dahn, Studies of lithium intercalation into carbons using nonaqueous electrochemical cells, Journal of The Electrochemical Society 1990,137.
9. T. Ohzuku, Y. Iwakoshi, and K. Sawai, Formation of lithium?graphite intercalation compounds in nonaqueous electrolytes and their application as a negative electrode for a lithium ion (shuttlecock) cell, Journal of The Electrochemical Society 1993, 140 , 2490.
10. Z. X. Shu, R. S. McMillan, and J. J. Murray, Electrochemical intercalation of lithium into graphite, Journal of The Electrochemical Society 1993, 140 922.
11. H.-P. Boehm, R. Setton, and E. Stumpp, Nomenclature and terminology of graphite intercalation compounds (iupac recommendations 1994), Pure Appl. Chem. 1994, 66 1893.
12. Wenlong Guo, Hongji Li, Mingji Li, Wei Dai, Zhou Shao, Xiaoguo Wu, Baohe Yang Synthesis of nickel nanosheet/graphene composites for biosensor applications,Carbon, 2014,79, 636-645
13. Mikael Larsson, Wei-Chen Huang, Meng-Hsuan Hsiao, Yen-Jen Wang, Magnus Nydén, Shih-Hwa Chiou, Dean-Mo Liu , Biomedical applications and colloidal properties of amphiphilically modified chitosan hybrids, Progress in Polymer Science, 2013, 38(9), 1307-1328
14. N.N. Mobarak, A. Ahmad, M.P. Abdullah, N. Ramli, M.Y.A. Rahman Conductivity enhancement via chemical modification of chitosan based green polymer electrolyte, Electrochimica Acta, 2013, 92 (1), 161-167
15. Nathalie K. Guimard, Natalia Gomez, Christine E. Schmidt Conducting polymers in biomedical engineering, Progress in Polymer Science, 2007, 32 (8–9, 876-921
16. Ray S. S., Okamoto M.: Polymer/layered silicate nanocomposites: A review from preparation to processing. Progress in Polymer Science, 2003, **28**, 1539–1641
17. Liang L., Liu J., Gong X. Y.: Thermosensitive poly (Nisopropylacrylamide)- clay nanocomposites with enhanced temperature response. Langmuir, 2000, **16**, 9895– 9899.
18. Xia X. H., Yih J., D'Souza N. A., Hu Z. B.: Swelling and mechanical behavior of poly (N-isopropylacrylamide)/ namontmorillonite layered silicates composite gels. Polymer, 2003, **44**, 3389–3393.
19. Ebru Günister, Dilay Pestreli, Cüneyt H. Ünlü, Oya Atıcı, Nurfer Güngör, Synthesis and characterization of chitosan-MMT biocomposite systems, Carbohydrate Polymers, 2007, 67(3), 358-365
20. J. P. Zhang1,2, A. Q. Wang1* Synergistic effects of Na+-montmorillonite and multi-walled carbon nanotubes on mechanical properties of chitosan film eXPRESS Polymer Letters ,2009, 3(5) ,302–308
21. I. Leceta, P. Arana, P. Guerrero, K. de la Caba, Structure–moisture sorption relation in chitosan thin films , Materials Letters, 2014,18(1) 125-127

22. George Z. Kyzas, Dimitrios N. Bikiaris, Eleni A. Deliyanni Advanced low-swelling chitosan/graphite oxide-based biosorbents, Materials Letters, 2014, 128, 46-49

23. C. Paluszkiewicz, A. Wesełucha-Birczyńska, E. Stodolak-Zych, M. Hasik, 2D IR correlation analysis of chitosan-MMT nanocomposite system, Vibrational Spectroscopy, 2012, 60, 185-188

24. Ingrid Corazzari, Roberto Nisticò, Francesco Turci, Maria Giulia Faga, Flavia Franzoso, Silvia Tabasso, Giuliana Magnacca,Advanced physico-chemical characterization of chitosan by means of TGA coupled on-line with FTIR and GCMS: Thermal degradation and water adsorption capacity, Polymer Degradation and Stability, 2015,112, 19

25. Hengchong Shi, Dean Shi, Cong Li, Shifang Luan, Jinghua Yin, Robert K.Y. Li Preparation of functionalized graphene/SEBS-g-MAH nanocomposites and improvement of its electrical, mechanical properties, Materials Letters, 2014,133, 200-203

26. Chao Zhang,Weng Weei Tjiu,Wei Fan, Zhe Yang,Shu Huang and Tianxi Liu, Aqueous stabilization of graphene sheets using exfoliated montmorillonite nanoplatelets for multifunctional free-standing hybrid films via vacuum-assisted self-assembly, J.Mater.Chem. , 2011,21, 18011

27. Ahmed. M. Youssef, Hussein Abou-Yousef, Samah M. El-Sayed, Samir Kamel, Mechanical and antibacterial properties of novel high performance chitosan/nanocomposite films, International Journal of Biological Macromolecules, 2015, 76, 25-32

28. Mingwei Tian, Xiaoning Tang, Lijun Qu, Shifeng Zhu, Xiaoqing Guo, Guangting Han Robust ultraviolet blocking cotton fabric modified with chitosan/graphene nanocomposites, Materials Letters, Volume 2015, 145, 340-343

29. Jae Ha Lee, Jason Marroquin, Kyong Yop Rhee, Soo Jin Park, David Hui, Cryomilling application of graphene to improve material properties of graphene/chitosan nanocomposites, Composites Part B: Engineering, 2013, 45(1), 682-687

30. K.H Bodek, G.W Bąk Ageing phenomena of chitosan and chitosan–diclofenac sodium system detected by low-frequency dielectric spectroscopy, European Journal of Pharmaceutics and Biopharmaceutics, 1999, 48 (2), 141-148

31. Sung Kyu Jang, Jaeho Jeon, Su Min Jeon, Young Jae Song, Sungjoo Lee Effects of dielectric material properties on graphene transistor performance, Solid-State Electronics, 2015, 109, 8-11